



**The author(s) shown below used Federal funding provided by the U.S. Department of Justice to prepare the following resource:**

**Document Title:** Development and Assessment of Analysis Tools for Examination of Microscopic Fracture Surface Topology and Degradation for Evidence Physical Match

**Author(s):** Ashraf F. Bastawros

**Document Number:** 252785

**Date Received:** April 2019

**Award Number:** 2015-DN-BX-K056

**This resource has not been published by the U.S. Department of Justice. This resource is being made publically available through the Office of Justice Programs' National Criminal Justice Reference Service.**

**Opinions or points of view expressed are those of the author(s) and do not necessarily reflect the official position or policies of the U.S. Department of Justice.**

**U.S. Department of Justice  
Office of Justice Programs  
National Institute of Justice**

**Award Number** 2015-DN-BX-K056

**Project Title:**

Development and Assessment of Analysis Tools for Examination of Microscopic Fracture  
Surface Topology and Degradation for Evidence Physical Match

**Principal investigator:**

Ashraf F. Bastawros, Professor, Aerospace Engineering, Iowa State University, Ames IA  
bastaw@iastate.edu, Tel: 515-294-3039

**Submission Date:**

June 30, 2018

  
**Recipient Organization:** Iowa State University  
1138 Pearson Hall  
505 Morrill Road  
Ames, IA 50011-2103

**Recipient Identification No.:** 4282008

**Project/ Grant Period:** January 1, 2016 – September 30, 2018

**Reporting Period End Date:** June 30, 2018

**Reporting Term:** Final Summary Overview

**Signature of Submitting Official:**

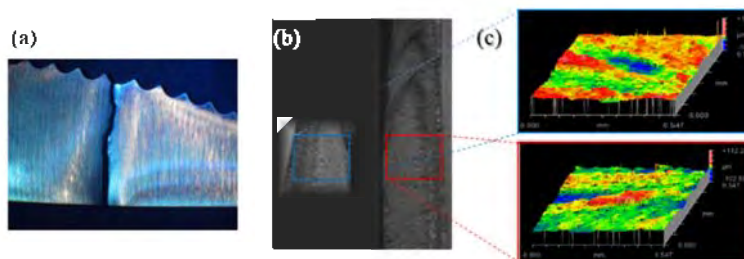
 7/2/2018

Ms. Marva Rutherford, MS, CRA; Senior Award Administrator  
Office of Sponsored Programs Administration Iowa State University

## 1. Purpose of Project:

The purpose of this project was to develop a science-based measurement and mathematical correlation algorithm for the forensic analysis of fracture surfaces. The *methodology* utilizes computer-based three dimensional (3D) spectral analysis of the fracture surface topography, mapped by a white light non-contact surface profilometer to provide an objective measurement of the similarity between fracture surfaces. Our methods use statistical learning tools trained on databases of both matches and non-matches. The proposed quantitative forensic comparisons have potential applications across a broad range of fractured materials and/or toolmarks, with diverse textures and mechanical properties. The developed framework will assist the examiner by providing analytical and statistical support for his/her decision, by estimating with confidence bounds the probability of a true match, and helping to arrive at a quantitative match decision.

**Fig. 1:** Association of fragments. (a) Visual jig-saw match of the macroscopic crack trajectory. (b) Comparative microscopy pattern matching. (c) 3D representation of fracture surface, showing detailed topographic features at relevant scale.



## 2. Project Design, Methods, and Data Analysis:

3D microscopy is utilized to enable the z (height) measurement at every x-y positions of the fracture surfaces within the field of view. As compared to typical feature counts by comparative microscopy which amounts to be in the tens of features, this method will provide thousands of surface points for comparison as shown in Fig. 1. The frequency of features occurring can be assessed and correlated mathematically. Some features will be class characteristics that are common to all the knives tested (same material and processing conditions). Some features (frequencies) are attributed to the rapid fracture and the fracture sequence for the individual knife. The result is a decision with quantified confidence.

### 2.1 Sample Generation:

The examined sample sets were selected to reflect variability in manufacturing processes, material microstructure and the random fracture events encountered in a crime scene. The first group of samples

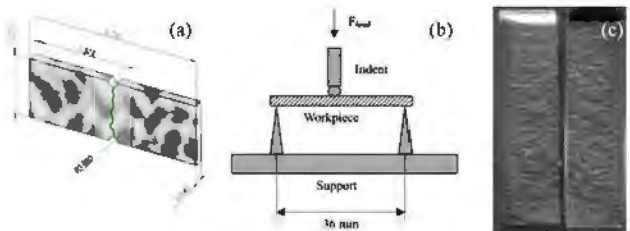
comprised 20 knives of the same brand and model, purchased from the manufacturer, Chicago Cutlery, to minimize variability in the manufacturing process. They were single serrated edged knives, approximately 21 cm in length as shown in Fig 2(a). Two sets of samples, 9 each, were fractured at random using a controlled bend fixture, shown in Fig. 2(b). The handles of the knives were cut off leaving approximately 5.5 cm of the blade from base to tip as shown in Fig. 2(a). For clarity, the surface attached to the knife handle is referred to as the “base” and the surface from the tip portion of the knife is referred to as the “tip”. The tips were then inserted into a vice about 2.5 cm. Using a pair of vice grips, each sample was bent to 60 degrees. Most samples fractured at that point, although some required to be bent back the other direction and usually fractured at approximately 30 degrees. The knife fractured into two pieces (labeled as the base and the tip). Once fractured, every sample was handled with gloves, taking care not to touch or damage the fracture surface in anyway.

**Fig. 2:** Knives samples testing protocol. (a) 10 fracture pairs of knives from the same patch. (b) Control bend fixture.



The second group of samples comprised 440 Stainless steel blocks (similar to the knives materials), water jet cut into a set of tensile test rods and a set of bend rods. This set underwent a controlled fracture in a universal testing frame, Fig. 3. Both the knives and the test rods have an average grain size of  $d_g = 25 - 35 \mu m$ . The knife and rod materials have a microstructure of ductile iron rich phase mixed with a brittle carbide phase.

**Fig. 3:** (a) Stainless steel sample testing protocol. (a) Waterjet cut rods with precursor notches. (b) 3point bend configurations. (c) Optical comparative microscopy of fracture surfaces pair.



## 2.2 Surface Characterization:

The pairs of fracture surfaces were imaged by a standard non-contact 3D optical interferometer (Zygo-NewView 6300), which provides a height resolution of 20 nm and spatial inter-point resolution of 0.45  $\mu m$  (Fig. 4a). Each of the base and tip fragments were mounted in a molding compound for manipulation and

alignment under the microscope (Fig. 4b). Each of the base and tip were inserted together on the microscope stage to ensure alignment and correspondence of images on the pairs of fragments. Figure 4(c-f) shows a pair of fracture surfaces, with 3D topological rendering and the corresponding 2D color map representations.

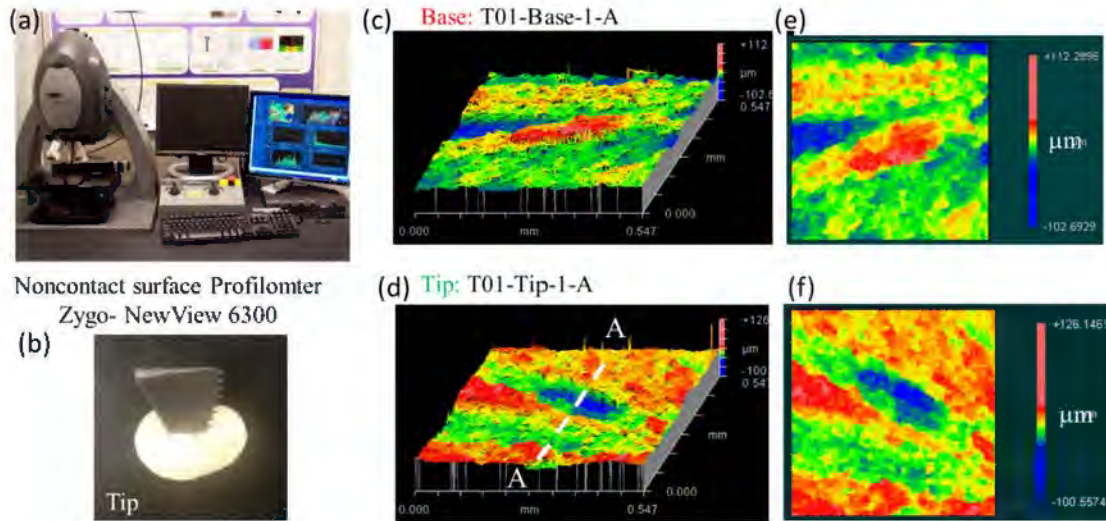
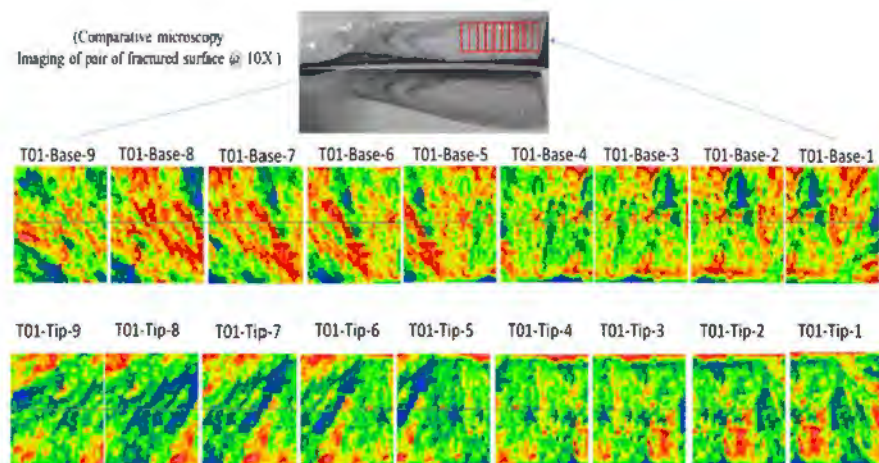


**Fig. 4:** Fracture surface characterization. (a) 3D surface profilometry. (b) Sample mounting. (c-f) Pair of fracture surfaces, shown in 3D perspectives and in 2D color map representations.

A set of nine surface height 3D topological images were collected on each fracture surface. These high-resolution images of 992x992 pixels, utilizing a single field of view at 20X magnification (550x550μm field of view) were used to perform the comparison between different pairs of images. The nine images were taken with a 75% overlap between adjacent surfaces as shown in Fig. 5 for the pairs of fracture surfaces for T01 tip and T01 base pieces. The rationale of utilizing these number of images and their overlap is to generate a full independent three images (Images 1, 5, 9) and to examine the minimum set of images and their characters required for discrimination analysis as will be discussed in the result section.

**Fig. 5:** A sample set of collected 9-images on a pair of the fracture surface.



For an illustration of the analysis protocol, a spatial height distribution in any desired direction can be generated (Fig. 6.b) from the 3D contour heights. Here the height distribution along line A-A in Fig 4(d) is shown in Fig. 6(a). The corresponding spectral representation (its mathematical Fourier representation in the frequency space) is shown in Fig. 6(b). The spectral analysis of such 2D data set can be split into its low-frequency component (green line on Fig 6(a)) representing the macro-fracture characteristics and unique river marks. The high frequency component (blue line) would be akin to grain size distribution. These details have the potential to provide a discriminating distribution of features on the surface. For example, these details are vividly quantized on the frequency spectra of Fig. 6(b) where in the low frequency portion represent the river marks on the fracture surface. Similarly, the grain size is represented in the middle frequency range, and the micro-fracture dimpling represents the high-frequency portion of the spectral map.

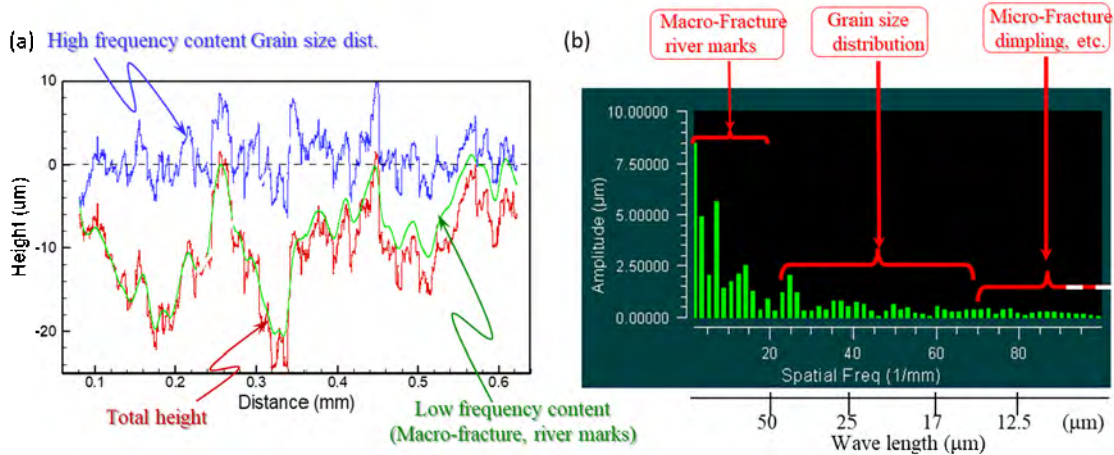


**Fig. 6:** Illustration of the spectral analysis of the topographic fracture surface of Fig. 4. (a) representation of the middle line of the image of Fig. 4(d) as a total height and the corresponding short and long wavelength information, revealed by Fourier analysis. (b) The corresponding frequency spectra of the 2-D line showing different topographic signatures.

For the utilized analysis in this work, the surface height 3D topographic maps were quantized using spectral analysis as summarized in Fig. 7 for a fracture surfaces of the stainless-steel samples. The two-dimensional (2D) fast Fourier transform (FFT) mathematical operator was applied to each image to calculate its spectral frequency distribution. Figure 7(b) shows the 2D FFT quantized image analysis in the spectral domain for a pair of images taken from a pair of fracture surfaces for T01 tip and T01 base pieces. After calculating the spectra of each pair of images, each spectrum was divided into multiple radial sectors as shown in Fig.

7(b). The segmented angular sectors for the frequency range ( $0^\circ$ ,  $180^\circ$ ) will represent the entire data set, because the frequency space representation exhibits inversion symmetry. The spectral array size is proportional to  $2^n$  as this is a mathematical feature of the FFT. For the image size we are utilizing in this work, this will yield a spectral array of 512 by 1024. The radial segments for comparison are chosen to reflect

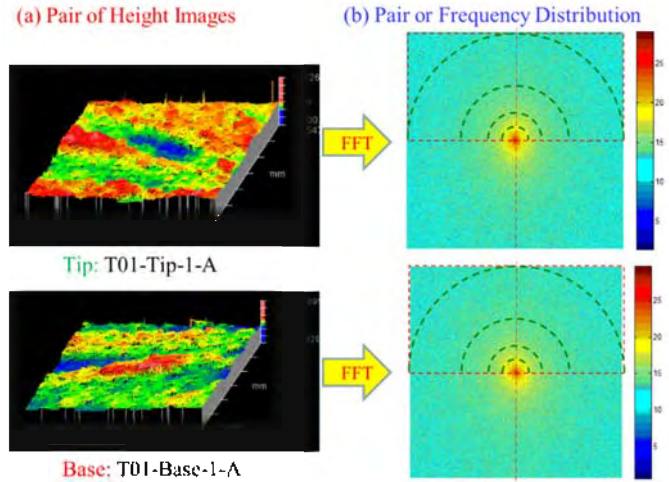


**Fig. 7:** Spectral representation of the 3D topological images, to be mathematically correlated for matching decision.

the physical process scales and the corresponding wavelength. The spectral analysis computational algorithms have been implemented and tested on Intel(R) Xeon(R) CPU E3-1270 v3 processor with 3.50 GHz speed, 16 GB RAM, and updating the algorithms to MATLAB R2017 environment.

### 2.3 Physical Matching by Spectral Analysis and Image Correlation Algorithm

The analysis begins by identifying the degree of similarity between the two spectra of the fracture pairs, and developing a representative measure for the degree of matching. For comparison, the correlation between the spectra from corresponding images on the tip and the base surfaces in different radial frequency bands between  $5 - 300mm^{-1}$  were calculated. Image pairs for when the tip and base surfaces were from the same knife are *true matches* while those pairs for when the tip and base surfaces were from different knives are true *non-matches*. For comparison, one can examine each feature independently, though an overall classification rule is constructed based on the probability density functions of all feature classes.

The topological height distribution of the fracture surface acquired from the 3D surface profilometer (Fig. 7.a), can be represented by a function:

$$\text{Height Distribution} = h(x, y); \quad \begin{cases} x = 1, N \text{ and } N \text{ is the number of pixel in } x\text{-dn} \\ y = 1, M \text{ and } M \text{ is the number of pixel in } y\text{-dn} \end{cases} \quad (1)$$

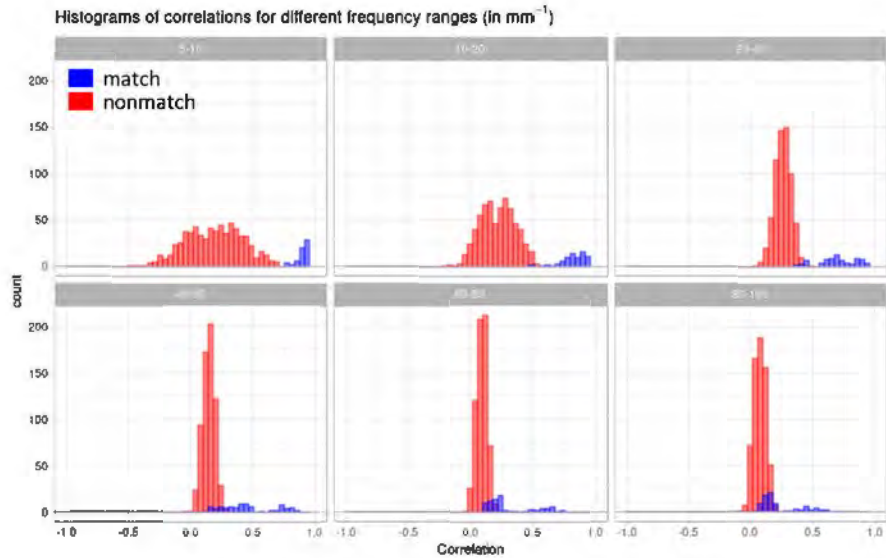
The measured height distribution function  $h(x, y)$ , defines the topology of the fracture surface at every spatial point,  $(x, y)$  on the fracture surface. Each wavelength on the fracture surface has a population,

$H(f_x, f_y)$  on the frequency domain, which is acquired from the mathematical FFT operator. With FFT operation, we get a representative map of the topological frequency component distribution;

$$\text{Frequency Distribution} = H(f_x, f_y); \quad \begin{cases} f_x = 2\pi/n; & n = 1, N/2 \\ f_y = 2\pi/m; & m = 1, M/2 \end{cases} \quad (2)$$

For example, grain size does not have a single frequency content within the spectrum, but rather has a distribution. Similarly, other microscopic fracture details would have a range of spectral distribution. The first step of the analysis was to identify the scale of the significant features of each image pair and their distributions. For a pair of fracture surfaces, the population of these features will contain relevant information about the physical processes present at each length-scale.

**Fig. 8:** Cross-correlations for individual images in matching and non-matching surfaces for two different sets of 9 knives with 9 images per knife. True matches and true non-matches can be distinguished in this example by features in two frequency ranges; 5-10 and 10-20 $\text{mm}^{-1}$ , while at higher frequencies the separation is less clear and begin to show substantial overlap.



The corresponding spectral power distribution function will be  $P(f_x, f_y)$ . To compare two fracture pieces, two-dimensional statistical cross-correlations between their power spectral density,  $P(f)$  (square of the frequency) for each surface spectral frequency,  $H(f)$  are computed in banded radial frequency, with increments in the bands determined by the scale of the image and type of material, yielding a similarity measure on each frequency band for the pairs of images. This is done for images from matching fracture surfaces and non-matching fractures in order to estimate the distribution for both the population of true matches and true non-matches.

To illustrate the discrimination strength of the methodological framework, Fig. 8 shows the comparison of 9-pairs of fractured knives, each separated to a base and a tip. 9-images were collected from each fracture surface (Fig. 5), resulting in 162-total images. In this example, image pairs for when the tip and base surfaces were from the same knife are true matches, while those pairs for which the tip and base surfaces were from different knives are true non-matches. Correlation analysis showed clear separation (with generally lower values for the true non-matches and higher values for the true matches) for the 5-10 and 10-20mm<sup>-1</sup> frequency band range, as shown in Fig. 8. Beyond these frequency ranges, the correlation histogram of the true matches and the true non-matches begin to be less distinctive from each other and started to overlap. This illustrates the commonality in the micro-mechanisms of the fracture process at the sub-grain level, as shown in Fig. 6(b). The classification and matching process is carried out in two steps; (a) Model training on an initial data set and (b) performing classification of new sample(s).

**(a) Model training and fitting:** The cross-correlations in specific frequency bands appear to distinguish fracture surfaces, so modeling the behavior of these correlations in those frequency bands in the population of matches and non-matches can be used to develop a rule for identifying corresponding fracture surfaces.

The modeling strategy is as follows:

1. Produce a set of fracture surface pairs and image them.
2. Compute the cross-correlations for sets of images from the matching and non-matching surfaces.
3. Transform the data using an appropriate variance-stabilizing transformation for correlation data, specifically, the Fisher z-transformation.
4. Fit models to describe the distribution of true matches and true non-matches, accounting for the difference in the correlations location and account for the correlation of repeated observations across the surface.

The matrix-variate Gaussian distribution is used to describe each class.

**(B) Classification of a new object:** A new pair of surfaces that have been imaged generates a matrix of observations  $X$  containing the transformed correlations of the images in those frequency bands. Presuming prior probability of being a true match  $p_1$ , and the prior probability of being a true non-match  $p_2 = 1 - p_1$ ,

the model learned previously assigns a probability of being a match by combining prior probabilities and the densities from the model:

$$P(X = match) = \frac{p_1 f_1(X)}{p_1 f_1(X) + p_2 f_2(X)} \quad (3)$$

where  $X$  is the set of transformed correlations from the frequency bands chosen for the class of materials in question for the  $k$ -aligned images from the sample,  $f_1(X)$  is the estimated probability density function for the true matches and  $f_2(X)$  is the estimated probability density function for the true non-matches. The results will typically be expressed as a log-odds ratio, which can be directly converted to a probability if desired. However, if the prior probabilities are equal, the log-odds ratio is equivalent to the log of a likelihood ratio. These probability density functions can also be used to create a classification rule rather than a probabilistic determination by combining the results with the cost of misclassification.

### 3. Results and Findings

The rough and irregular metallic fracture surfaces carry many details of the metal microstructure as well as its loading history. The discrimination algorithm has the power for object classification for all fracture pairs, regardless of their point of origin. Figure 9 shows an example of classification using models trained on sets of 9 knives with  $k=9$  images taken per knife, and an equal prior and then tested on two sets of 9 knives, one of which was imaged three times (labeled “K-9-06 rep 1”, “K-9-06 rep 2”, “K-9-06 rep 3”, and “K-9-9-01”) and two sets of 10 steel surfaces (labeled “S-10-9-10-01” and “S-10-09-02-01”) with the output given in terms of the log-odds of being a match - log-odds larger than zero indicate classification as a match. Each set of knives has 9 true matches and 72 true negatives and each set of steel samples has 10 true matches and 90 true negatives. Each of the six models were tested against all six sets, making a total of 336 possible true matches and 2808 possible true negatives. The fitted models have a 0.6% false negative rate (2/336) and a 0% false positive rate (0/2808). The two false negatives were from two different models failing to classify one specific knife base-tip pair correctly due to poor quality original topological images.

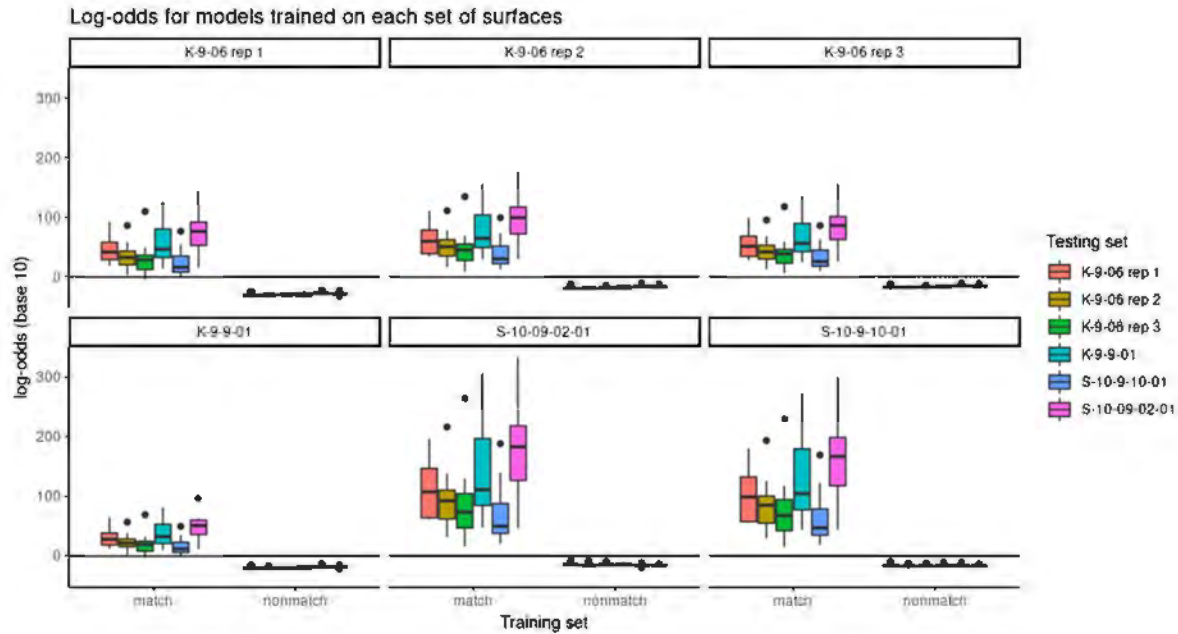


**Fig. 9:** The log-odds (base 10) for classifiers trained, using 9 images per knife, on each set of 9 knives and tested on each set of knives. Log-odds greater than 0 indicates classification as a match. In each set there are 9 true matches and 72 true non-matches. The 9-image models have a 0.6% false negative rate (2/336) and a 0% false positive rate (0/2808).

The results of the discrimination analysis based on fewer images are summarized in table 1. Models were trained using the full set of  $k=9$  images per knife and then tested against all possible subsets of a given size, from  $k=2$  to 9 images, with the parameters of the full model appropriately restricted to match the configuration of images being tested. In these data sets, using five or more images was

# of Images	False Positive Rate	False Negative Rate
2	0.00132 (133)	0
3	0.000254(60)	0
4	0.000017(6)	0
5	0	0
6	0	0
7	0	0.000165(2)
8	0	0.00298(9)
9	0	0.00595(2)

Table 1: Error rates and total number of erroneous cases by number of images

sufficient to attain a 0% false positive rate and using six or fewer images attained a 0% false negative rate (increasing the number of images of poorly captured features on the surface). The highest false negative rate was 0.6% (using all 9 images) and the highest false positive rate was 0.13% (using 2 images). In the cases of true matches, 99.1% of cases provided “extremely strong” evidence of a match (likelihood ratio  $>10^6$ ) and, similarly, in cases of true non-matches strong evidence of a non-match occurred in 87.5% of all cases. The distance from being misclassified among the true non-matches was a monotonically increasing function of the number of images used in the testing set (that is, the worst-case scenario improved as the number of images increased). However, the converse was not true for the true matches.

#### **4. Implications for criminal justice policy and practice in the United States**

The study responds to a need for advanced methods that aid in the analysis and comparison of fracture and torn surfaces. This has been expressed by trace evidence analysts in federal, metro-area and small forensic laboratories. The machine-based computational methodology will provide a quantitative assessment of fracture surfaces for forensic comparison, combined with a statistical expression of the comparison. Such a protocol is expected to enhance the ability of forensic scientists to capture, visualize and analyze fracture patterns, and to express the likelihood of a match between patterns in statistical terms that support the qualitative and quantitative judgment of the examiner. Successful advancement of the project technique has the potential to provide a new investigative machine-based analysis with quantified error probabilities that can be applied in performing physical matches for a variety of materials.

#### **5. Scholarly Products:**

1. 3PhD students, 1MS and 4-undergraduate REU
2. A. Bastawros, (Invited Talk) Application of Fracture Mechanics to the Forensic Match Analysis IMECE, Phoenix, AZ, 13-17, 2016.
3. A. Bastawros; X. Shang; B. Lograsso; T. Yu; H. Wang; J Vanderkolk, "Utilization of Spectral Analysis for Comparison of Fracture Surface Topology," Society of Experimental Mechanics Meeting, Indianapolis IN, June 12-15, 2017.
4. R. Maitra; A. Bastawros; B. Dawood; N. Garton; B. Lograsso; W. Meeker; G. Thompson; J Vanderkolk, "Fracture Mechanics-Based Quantitative Matching of Evidence Fragments," 2017 International Forensic Science Error Management Symposium, NIST, Gaithersburg MD, July 24-27.
5. Dawood, B., Thompson, G., Lograsso, B., Bastawros, A., Meeker, W., Maitra, R., Vanderkolk, J. "Fracture Mechanics-Based Quantitative Matching of Forensic Evidence Fragments: (A) Methodology and Implementation," Impression Pattern & Trace Evidence Symp. (Jan. 22-25, 2018) Arlington, VA.
6. Dawood, B., Thompson, G., Lograsso, B., Bastawros, A.F., Meeker, W., Maitra, R., Vanderkolk, J. "Fracture Mechanics-Based Quantitative Matching of Forensic Evidence Fragments: (B) Statistical Framework," Impression Pattern and Trace Evidence Symposium (Jan. 22-25, 2018) Arlington, VA.
7. A.F. Bastawros PODCAST (2018): Just Fracture Matches; Dr. Bastawros discusses how fracture mechanics principles can be used with statistical learning tools to give quantitative results. 2018 IPTES: Just Fracture Matches, <https://forensiccoe.org/js3e2/>
8. J.V. Vanderkolk, "Fracture Examination Research and Generalization of Examinations," AFTE 2018 49th Annual Training Seminar, June 3-8, 2018 Charleston, WV.
9. A.F. Bastawros, B. Dawood, N. M. Garton, B.K. Lograsso, R. Maitra, W. Q. Meeker, G. Z. Thompson, J. Vanderkolk, T. Yu, Fracture Mechanics Based Framework for Quantitative Physical Match Analysis of Evidence Fragments, (in preparation for PNAS).
10. B. Dawood, G. Z. Thompson, T. Yu, B.K. Lograsso, R. Maitra, W. Q. Meeker, J. Vanderkolk, A.F. Bastawros, Microscopic Examination of Fracture Surface Topology for Physical Match Analysis, (in preparation for AFTE Journal-July 2018).
11. G. Z. Thompson, et. al., Discriminant Analysis for Matrix-Variate Normal and t-distributed Random Variables, (in preparation for Technometrics -July 2018).